

# Effect of Inclusion and Filtration on Grain Refinement Efficiency of Aluminum Alloy



JIawei YANG, YIJIANG XU, SARINA BAO, SHAHID AKHTAR, ULF TUNDAL, STIG TJØTTA, and YANJUN LI

It is well known that the filtration efficiency of ceramic foam filters (CFF) on aluminum melt can be significantly reduced by the addition of grain refiner particles under a high inclusion load. Also, it is usually considered that the filtration process has little impact on grain refinement efficiency. In this work, the influence of inclusions and filtration on the grain refinement effect of AA 6060 alloy has been studied. This was done through TP-1 type solidification experiments where the aluminum melt prior to and after the filter during a pilot-scale filtration test was investigated. In the experiments, 80 PPI CFFs were used to filtrate aluminum melt with an ultra-high inclusion load and two addition levels of Al-3Ti-1B master alloys. It is found that both inclusions and filtration significantly reduce the grain refinement efficiency of the grain refiner master alloys. A detailed characterization of the used filters shows that the reduction of grain refinement efficiency is due to the strong adherence of TiB<sub>2</sub> particles to the oxide films, which are blocked by the CFF during filtration. A grain size prediction model based on deterministic nucleation mechanisms and dendritic growth kinetics has been applied to calculate the solidification grain size and estimate the loss of effective grain refiner particles during filtration. It is shown that due to the strong adherence between TiB<sub>2</sub> particles and oxide films in the melt, the high addition level of aluminum chips also has an influence on reducing the grain refinement efficiency of aluminum melt without filtration. The results of this study extended our understanding of the behavior and performance of inoculant particles in CFF and their interactions with the inclusions.

<https://doi.org/10.1007/s11661-021-06570-5>  
© The Author(s) 2022

## I. INTRODUCTION

FOR Al alloys, grain refinement by addition of effective grain refiners can significantly reduce the grain size of the alloys, resulting in an increase in mechanical properties, castability, and structural homogeneity.<sup>[1-7]</sup> The final solidification grain size of aluminum alloys is controlled by nucleation and growth of the grains. To achieve fine equiaxed grains, it is important to maximize the number of potent nucleation sites and restrict the growth of the grains. It is widely accepted that the grain refiner particles act as nucleation substrates, which significantly increases the nucleation rate of Al grains. Greer *et al.*<sup>[3,8,9]</sup> proposed that the nucleation of Al

grains on inoculant particles is an athermal process, based on which a free growth model is built. The free growth model suggested that the free growth undercooling of grains depends on the size of inoculant particles and the available undercooling in melt, regardless of time. Based on the free growth model, a grain size prediction model for inoculated aluminum alloys has also been proposed by Greer *et al.*,<sup>[3]</sup> by taking into account the effects of cooling rate, the concentration of solute elements, and the amount of added inoculant particles. In the model, the growth kinetics of grains is based on an assumption of spherical-shaped grains while the nucleation process stops because of recalescence. This model has been used to predict the grain size of as-solidified TP-1 test samples, showing a good agreement with the experimental results. Recently, Du and Li,<sup>[10]</sup> and Xu *et al.*<sup>[1,11,12]</sup> have developed new grain size prediction models of inoculated aluminum alloys based on the free growth model, by including the solute segregation stifling effect and temperature gradient effects on nucleation. The latest model<sup>[11,12]</sup> also includes the dendritic growth kinetics and globular to dendritic transition (GDT) of grains. Such models have been well validated by *in situ* X-ray radiographic solidification

---

JIawei YANG and YANJUN LI are with the Norwegian University of Science and Technology, 7491 Trondheim, Norway. Contact e-mail: yanjun.li@ntnu.no YIJIANG XU and SARINA BAO are with the SINTEF Industry, 7465 Trondheim, Norway. SHAHID AKHTAR is with the Research and Development Karmøy, Norsk Hydro, 4265 Håvik, Norway. ULF TUNDAL and STIG TJØTTA are with the Hydro Aluminum Primary Metal, Commercial Technology, Romsdalsvegen 1, 6600 Sunndalsøra, Norway.  
Manuscript submitted September 3, 2021; accepted: December 3, 2021.

experiments with different constant cooling rates and temperature gradients, showing excellent predictability in terms of grain size, maximum nucleation undercooling, and solid fraction at nucleation ceasing.

Nowadays, the Al–Ti–B type grain refiners are commonly used in the Al industry as they can provide high potency TiB<sub>2</sub> particles acting as heterogeneous nucleation sites for Al grains. It is well known that the grain refinement efficiency of a grain refiner master alloy can be severely affected by the poisoning effect and fading effect. For example, Zr poisoning<sup>[13]</sup> often occurs in different Zr-containing Al alloys where the Al–Ti–B type grain refiners were used. A presence of 100 ppm Zr in the aluminum melt can cause the formation of a Ti<sub>2</sub>Zr layer that will replace the Al<sub>3</sub>Ti layer on the (0001) crystal planes at the surface of TiB<sub>2</sub> particles. Such a replacement causes an increase in lattice misfit from 0.09 to 4.22 pct with {111} planes of aluminum. Si has a similar poisoning effect<sup>[14]</sup> on grain refinement when the Si concentration exceeds 3.5 wt pct in Al–Si based alloys. In addition to the poisoning of grain refiners, the fading effect of grain refiners is also known to reduce the grain refinement efficiency.<sup>[15–17]</sup> In previous research by the authors,<sup>[17]</sup> the agglomeration and sedimentation of grain refiners have been studied. It was found that inoculated commercial purity aluminum has a much larger grain size after 4 hours of settling than the alloy melts without settling. This is mainly owed to the agglomeration and sedimentation of the grain refiner particles in the melt, which causes a decrease in the number density of effective nucleation sites. It was also found that TiB<sub>2</sub> particles tend to adhere and agglomerate onto the oxide films in the aluminum melt when many aluminum chips are added to the melt.

The use of recycled aluminum alloys has become more important in the aluminum industry nowadays. Compared to the energy-costly primary aluminum production process, recycling of aluminum has a large benefit in several aspects, such as energy-saving, reduction of solid waste disposal, and reduction of greenhouse gas emissions.<sup>[18]</sup>

Filtration by ceramic foam filter (CFF) is a commonly used method in the Al industry to physically separate the unwanted solid inclusion particles from the liquid melt. Generally, the physical separation by filter is mostly through three different modes, sieving mode, cake mode, and depth mode.<sup>[19–21]</sup> The sieving mode occurs when the inclusions are larger than the filter windows, which makes them not able to pass through and thereby become retained in the filter medium. When the sieving mode occurs and the filtration process continues, the gradually accumulated inclusions will form a cake layer at the surface of the filter. This cake layer will cause a reduction in the effective pore size of filter and hence increase the filtration efficiency. At this stage, the filtration mechanism changed from the sieving mode to the cake mode. When the inclusions are smaller than the filter window, they can still be filtrated by the filter by the so-called deep bed mode or depth mode. This occurs inside the filter, and the inclusions are retained in the filter mainly because of the complicated structures of the filter.

It has been widely reported that the addition of grain refiner will cause a decrease in filtration efficiency for 50 PPI CFF under the “high inclusion load”.<sup>[22–24]</sup> A comprehensive study about the mechanisms behind this phenomenon has been done in an earlier work by the present authors.<sup>[25]</sup> It is found that with an addition level of 0.5 kg/ton grain refiner, the filtration efficiency of both 50 PPI and 80 PPI CFF is not affected, regardless of the inclusion load. However, when the grain refiner addition level was increased to 2.0 kg/ton, the detrimental effect starts to appear for 50 PPI filter under an ultra-high inclusion load. Interestingly, when 80 PPI filter is used for filtration of a melt with an ultra-high inclusion load, the addition of the same amount of grain refiner does not affect the filtration efficiency anymore. This has been attributed to the oxide film effects on blocking inclusions in the filter. However, how this strong adherence influences the grain refinement efficiency of the grain refiner master alloys is still unclear.

It is usually considered that the filtration process does not affect the grain refinement of aluminum alloys during solidification. To the knowledge of the present authors, how and to what degree the filtration process affects the grain refinement efficiency, especially for aluminum melt with an ultra-high inclusion load, has never been reported.

In this work, a systematic investigation about how filtration affects the grain refinement efficiency under an ultra-high inclusion load condition has been conducted; 80 PPI filters have been used to filtrate aluminum melts containing an ultra-high inclusion load and different amounts of grain refiners. The 80 PPI filter and ultra-high inclusion load are chosen to amplify the filtration effects on the grain refinement efficiency. By comparing the grain structure of aluminum alloys with and without inclusion additions, solidified under the same cooling rate before and after filtration, the effect of filtration and inclusions in the melt on the grain refinement efficiency is quantitatively studied. A grain size prediction model has been used to predict the grain size and estimate the loss of potent grain refiner during the filtration process.

## II. EXPERIMENTAL

### A. Materials

The experimental materials used in the present work include an AA 6060 alloy, Al–3Ti–1B master alloy in the form of a rod, and chips of AA 6060 alloy as the inclusion source. The AA 6060 chips are added into the 6060 alloy melt in the form of blocks with a height of 5.5 cm, width of 6 cm, and length of 15 cm, with a weight of approximately 1 kg per block. All materials are provided by Hydro Aluminum (Sunndalsøra, Norway), while the 80 PPI CFF with dimensions of 584 × 584 × 50 mm was provided by Pyrotek (Grevenbroich, Germany). The filter used contains > 70 wt pct aluminum oxide, 0.5 to 1.5 wt pct bentonite, and 1 to 10 wt pct aluminum phosphate. The chemical composition of the AA 6060 alloy used is listed in Table I.

**Table I. Chemical Composition of AA 6060 Alloy**

Compositions	Si	Fe	Cu	Mn	Mg	Ti	Al
Wt Pct	0.4	0.17	0.001	0.11	0.4	0.01	bal.

The 80 PPI filters have an excellent filtration efficiency due to their fine pore size. A smaller pore size also causes an easier formation of bridges by the oxide films. Therefore, the 80 PPI filter is suitable for the study of how inclusions and the filtration process affect grain refinement efficiency, even though it is not the most commonly used filter in the industry nowadays.

### B. Experimental Process

A schematic loop of the filtration experiment used in the present work is shown in Figure 1; 9.0 tons of 6060 alloy was first melted in a melting furnace. The liquid metal flowed from the outlet of the casting furnace into the launder and then flowed through the filter box and returned to the casting furnace in the end. The metal pump was used to control the flow rate of the melt, approximately 7 ton/h. The metal temperature in launder was measured and held at approximately 730 °C. The priming of 80 PPI filters was done by using the new Drain Free Filtration (DFF) technology developed by Hydro<sup>[26]</sup>; 80 kg of inclusion chip blocks was introduced into the melting furnace approximately 20 to 30 minutes after filtration started. Two Liquid Metal Cleanliness Analyzers (LiMCA) II were used and placed both before and after the filter as illustrated in Figure 1. The LiMCA II is able to detect inclusions in the melt and gives an on-line inclusion level analysis. An Al-3Ti-1B grain refiner rod was continuously introduced to the melt in launder approximately 10 minutes after the chip addition. TP-1 type solidification tests were conducted approximately 10 minutes after the addition of grain refiners started. A major difference between the standard TP-1 test<sup>[27]</sup> and the TP-1 type test<sup>[17,28]</sup> used in this work is that the latter one uses casting crucibles with different crucible dimensions and cooling conditions. Aluminum melt in the launder was taken both before and after the filter by using the pre-heated boron nitride coated steel crucibles with a wall thickness of 2 mm, height of 30 mm, and outer diameter of 33 mm at the top and 23 mm at the bottom of the crucible. During the solidification process, the crucibles were covered by insulation materials at both top and bottom to obtain a relatively homogeneous cooling rate for the whole sample. A well-calibrated K-type thermocouple was inserted in the central region of the crucible to measure the cooling curve of the sample during solidification. The recording rate was set to 50 Hz, which corresponds to 0.02 seconds per measurement. The TP-1 type solidification test was repeated three times for each sample.

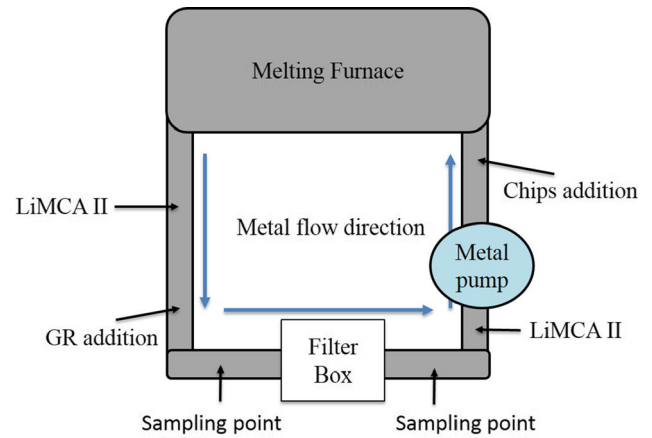


Fig. 1—Top view of the filtration loop used for the present work.

Samples for the Porous Disc Filtration Apparatus (PoDFA) test were also collected both before and after the filtration, at the same positions in the launder as for the TP-1 type tests. Approximately 1.5 kg of molten aluminum was sampled by a ladle and poured into the preheated PoDFA crucible, which had a filter with fine pores at the bottom. The liquid passes through the fine filter aided by the vacuum, and the residual liquid above the filter will have a higher concentration of the inclusions. After solidification, the samples highly concentrated with inclusions were sliced and analyzed to give the inclusion types and numbers in the melt.

Since the grain refiner was always added after the inclusion addition for the filtration test, the grain refinement efficiency of a clean AA 6060 alloy with grain refiners cannot be tested in the pilot-scale filtration experiments. Therefore, to further confirm the effect of inclusions on grain refinement, separate laboratory-scale experiments were carried out; 1 kg of AA 6060 alloy without any inclusion addition was melted in an alumina crucible in a muffin furnace. Al-3Ti-1B grain refiner master alloy, with 0.5 and 2.0 kg/ton addition levels, was introduced after the aluminum was fully melted at 730 °C. A carbon rod was used to stir the melt to disperse the grain refiner particles well. Then, TP-1 type tests were conducted on the inoculated aluminum melts with the same procedure.

The solidified TP-1 test samples were cut vertically in the center, ground, polished, electro polished with A3 electrolyte from Struers® at -35 °C with a voltage of 20 V for 45 seconds, and further anodized with 95 wt pct H<sub>2</sub>O + 5 wt pct HBF<sub>4</sub> solution at 20 V for 90 seconds for microstructure characterization under optical microscopy (MEF4M, LEICA, Wetzlar, Germany).

To ensure the accuracy of the grain size measurement, the grain structure was also characterized by scanning electron microscopy (SEM) (Ultra 55, Zeiss, Oberkochen, Germany) with a Nordif electron backscatter diffraction (EBSD) detector after the electro-polishing. TSI OIM software was used for the analysis of EBSD data. Table II shows an overview of the experiments.

**Table II. Overview of the Addition Levels of Inclusions and Grain Refiners of Different TP-1 Tests**

Sample	Inclusion Load (kg/batch)	CFF (PPi)	GR Addition Level (kg/ton)	Remarks
A	80	80	0.5	before filtration
B	80	80	0.5	after filtration
C	80	80	2.0	before filtration
D	80	80	2.0	after filtration
E	0	no filtration	0.5	clean 6060 alloy
F	0	no filtration	2.0	clean 6060 alloy

**Table III. Physical and Thermodynamic Parameters of Al–Si Alloy Used for Simulation**

Quantity	Symbol	Units	Value	References
Volumetric Latent Heat	$L$	$\text{J m}^{-3}$	$9.5 \times 10^8$	[3, 31]
Volumetric Heat Capacity of Liquid	$c_{p_l}$	$\text{J m}^{-3} \text{K}^{-1}$	$2.58 \times 10^6$	[3, 31]
Gibbs–Thomson Coefficient	$\Gamma$	$\text{M K}$	$1.96 \times 10^{-7}$	[32]
Solute Diffusivity in Al Melt	$D_1$	$\text{m}^2 \text{s}^{-1}$	$2.8 \times 10^{-9}$	[33]
Liquidus Slope	$m$	$\text{K wt pct}^{-1}$	$-6.6$	[5]
Partition Coefficient	$k$		0.11	[5]

### C. Simulation

The numerical model used in this work is based on the recently developed as-cast grain size prediction model,<sup>[10,11,29]</sup> where the grain growth model is based on dendritic growth kinetics of hemispherical-shaped dendrite tips.

For the TP-1 type solidification cases, the melt is assumed to be spatially isothermal and recalescence acts as the nucleation stifling mechanism. Therefore, the latent heat released during solidification, together with the external cooling rate, determines the changing rate of solid fraction. The thermal history of the melt is treated as a series of short temporally isothermal steps of duration  $dt$ . Then, the melt temperature in the next time interval  $T_{t+1}$  is related to the current temperature  $T_t$ , by:

$$T_{t+1} = T_t - \dot{T}dt + \frac{L \cdot df_s}{C_{p_v}} \quad [1]$$

where  $\dot{T}$  is the external heat extraction rate, usually taken to be the cooling rate before the onset of solidification,  $L$  the enthalpy of fusion per unit volume,  $C_{p_v}$  the heat capacity of melt per unit volume, and  $df_s$  the increment of solid fraction in each time step  $dt$ . The cooling rate is taken from the experimentally measured data.

The average linear intercept grain size in 2-D,  $\bar{D}$ , is calculated from the volumetric total grain number density  $N_{V,\text{tot}}$ <sup>[3,30]</sup>:

$$\bar{D} = \sqrt[3]{0.5/N_{V,\text{tot}}} \quad [2]$$

To simplify the solidification path during simulation, the experimental alloy investigated in the present work was treated as a binary Al–0.706 wt pct Si alloy, which has an equivalent growth restriction factor  $Q$  to AA 6060 (total  $Q$  is 4.15 K). The physical and thermodynamic parameters of Al–Si alloy used in the modeling are listed in Table III. The particle size distribution of  $\text{TiB}_2$  particles in Al–3Ti–1B is described by a log-normal distribution, assumed to be the same as the Al–5Ti–1B master alloy experimentally determined in a previous work,<sup>[11]</sup> where the total number of potent  $\text{TiB}_2$  particles per unit volume melt,  $N_0 = 2.5 \times 10^{11} \text{m}^{-3}$ , per 0.1 wt pct Al–3Ti–1B addition was used.

## III. RESULTS

### A. Impact of Filtration on Grain Refinement Under Ultra-High Inclusion Load

Figures 2(a) and (b) shows the microstructure of the solidified samples of TP-1 type tests for the alloys containing a high inclusion load with a grain refiner addition level of 0.5 kg/ton before and after filtration, which correspond to sample A and B in Table II, respectively. The inclusion level in the melt before filtration was measured as average N20 (number of inclusions  $> 20 \mu\text{m}$  in diameter)  $> 12 \text{k/kg}$  by using LiMCA, which is an ultra-high inclusion load. As can be seen, both alloys show an equiaxed grain structure. The grain size of the ingot for the post-filtration melt is larger than that before filtration. The average grain sizes in the two alloys are measured as 435 and 577  $\mu\text{m}$ , respectively, by using a liner intercept method. This indicates that the grain refinement efficiency is reduced by the filtration process.



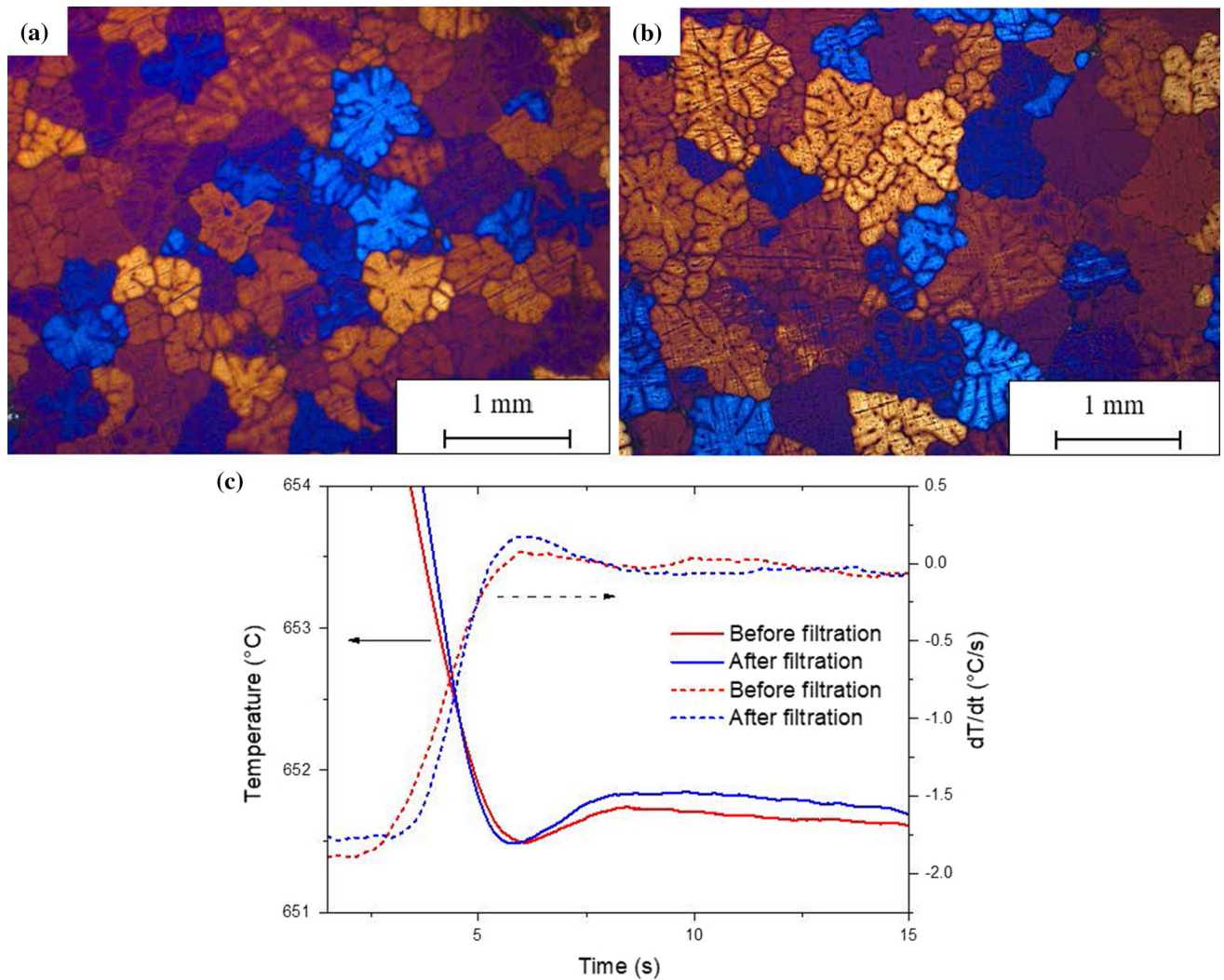


Fig. 2—Solidification structure and cooling curve for samples A and B from TP-1 type tests. (a) Solidified aluminum with a grain refiner addition level of 0.5 kg/ton before the filtration. (b) Solidified aluminum with a grain refiner addition level of 0.5 kg/ton after the filtration. (c) Cooling curve (solid lines) with the corresponding first derivative  $dT/dt$  (dashed lines) of Samples A and B.

Figure 2(c) shows the measured cooling curves (solid line), liquid temperature  $T$  as a function of solidification time, of TP-1 test samples and their corresponding first derivatives,  $dT/dt$  (dashed line) of samples A (before filtration) and B (after filtration), where the initial cooling rates are measured as approximately 1.6 and 2.0 K/s, respectively. The minimum nucleation temperature can be determined from the  $dT/dt$  curve when it shows a sharp increase. As can be seen, the nucleation starting temperature of alloy A is slightly higher than that of alloy B, which is in agreement with the grain structure. Clear recalescence can be observed in both cooling curves. However, little difference in maximum nucleation undercooling of the two samples can be detected.

Figures 3(a) and (b) shows the grain structure of TP-1 type test samples of ultra-high inclusion loaded melts with a grain refiner addition level of 2.0 kg/ton before and after filtration, corresponding to sample C and D, respectively. As can be seen, the grain size of sample C is smaller than sample A, which is grain refined by 0.5

kg/ton Al-3Ti-1B, showing the effect of increased grain refiner levels. However, after filtration, the grains in sample D become much larger, even larger than in sample B. The measured grain sizes of sample C and D are 401 and 816  $\mu\text{m}$ , respectively. This implies that the filtration has a more significant reduction effect on the grain refinement efficiency of melts with a higher addition level of grain refiners.

The measured typical cooling curves of samples C and D are shown in Figure 3(c). The initial cooling rate of sample C and D are 2.0 and 1.6 K/s, respectively. It can be seen that the maximum nucleation undercooling  $\Delta T_{n,max}$  of sample D is significantly higher than alloy C, indicating less effective inoculant particles existing in sample D than in sample C. This confirms that the grain refinement effect has been significantly reduced by the filtration.

Figures 4(a) and (b) shows the solidification grain structure of TP-1 test samples of clean AA 6060 alloy melts with 0.5 and 2.0 kg/ton addition levels of grain

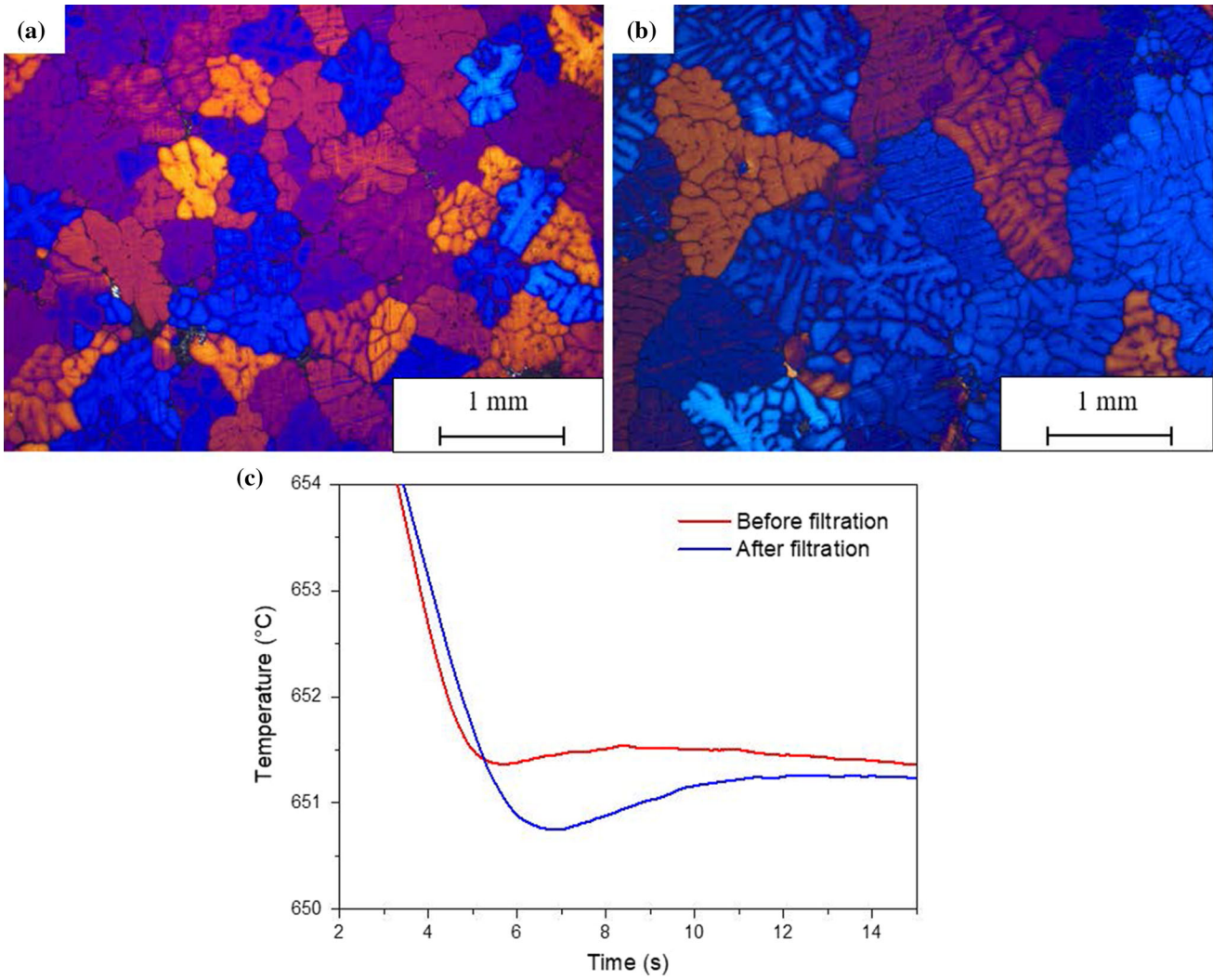


Fig. 3.—Solidification structure and cooling curve for samples C and D from TP-1 type tests. (a) Solidified aluminum with a grain refiner addition level of 2.0 kg/ton before the filtration. (b) Solidified aluminum with a grain refiner addition level of 2.0 kg/ton after the filtration. (c) Cooling curve of samples C and D.

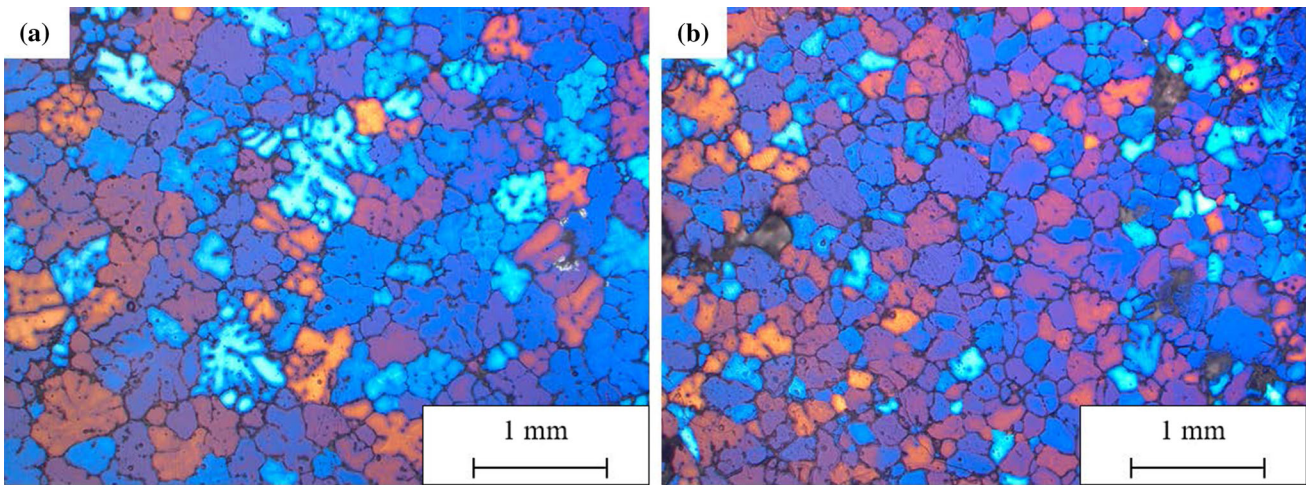


Fig. 4—Solidification structure for samples E and F from TP-1 type tests. (a) Solidified aluminum with a grain refiner addition level of 0.5 kg/ton and (b) for 2.0 kg/ton, without inclusion introduction.



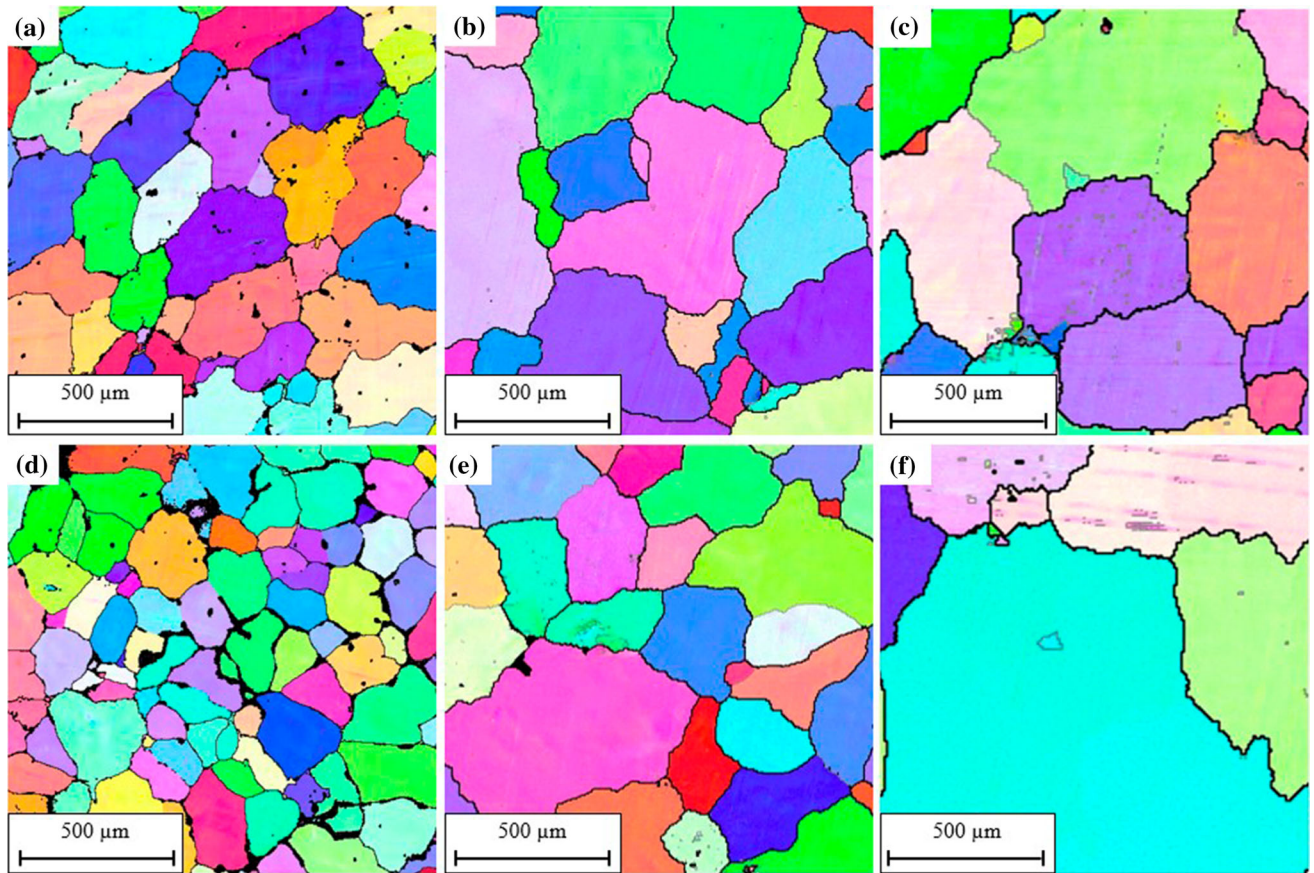


Fig. 5.—EBSD grain structure of solidified TP-1 test samples. (a) 0.5 kg/ton, GR without inclusions (sample E), (b) 0.5 kg/ton GR with chips before filtration (sample A), (c) 0.5 kg/ton GR with chips after filtration (sample B), (d) 2.0 kg/ton GR without inclusions (sample F), (e) 2.0 kg/ton GR with chips before filtration (sample C), (f) 2.0 kg/ton GR with chips after filtration (sample D). Black dots in the figures are due to porosities.

**Table IV. Measured Grain Size on Anodized Samples and EBSD Mapping Based on Interception Metho, and Predicted Grain Size by Modeling**

Sample	GR Addition Level (kg/ton)	Remark	Cooling Rate (K/s)	Grain Size Calculated or Measured ( $\mu\text{m}$ )		
				Anodized (OM)	EBSD	Modeling
A	0.5	before filtration	1.6	$435 \pm 63$	$340 \pm 23$	—
B	0.5	after filtration	2.0	$577 \pm 46$	$407 \pm 37$	—
C	2	before filtration	2.0	$401 \pm 44$	$286 \pm 14$	—
D	2	after filtration	1.6	$816 \pm 139$	$606 \pm 36$	—
E	0.5	no chip addition	2.0	$393 \pm 20$	$262 \pm 18$	239
F	2.0	no chip addition	1.6	$329 \pm 36$	$177 \pm 8$	191

The Uncertainty Corresponds to the standard Deviation.

refiner, corresponding to sample E and F, respectively. As can be seen, the grain size is much smaller in the sample inoculated by 2.0 kg/ton grain refiners that that with 0.5 kg/ton grain refiners. The measured grain sizes of sample E and F are 393 and 329  $\mu\text{m}$ , respectively. Compared sample A and C, the grain refinement efficiency is higher in the alloys (E and F) without addition of inclusions.

EBSD was also used to determine the grain size in the present work. Figures 5(a) through (c) shows the EBSD images of grain structures of TP-1 type test samples with

0.5 kg/ton grain refiner addition with (a) no inclusion (sample E), (b) with inclusion before filtration (sample A), and (c) with inclusion after the filtration (sample B). Similarly, Figures 5(d) through (f) shows the samples with 2.0 kg/ton grain refiner addition (d) without inclusion (sample F), (e) with inclusion before filtration (sample C), and (f) with inclusion after the filtration (sample D). The measured average grain sizes using the linear intercept method are included in Table IV. The measured grain sizes from the anodized samples by using OM images are always larger than those measured

from EBSD mapping. This is because it is often difficult to distinguish the color differences of some neighboring anodized grains under OM. Therefore, grain size measured by SEM-EBSD is supposed to be more reliable. Nevertheless, the grain sizes measured by EBSD confirm that inclusion in melt and filtration have reduced the grain refinement efficiency of grain refiners, and this reduction is more significant for the alloys with a higher addition level of grain refiners. Furthermore, the alloys without chip additions have less standard deviation in grain size measurement, indicating a more homogeneous microstructure.

### B. Modeling Results

Table IV shows a comparison between the grain size measured by the linear interception method using the anodized OM image samples, SEM-EBSD images, and predicted grain size. For the modeling result, since the impact of filtration and inclusion on grain refinement is unknown, the grain size after the filtration cannot be predicted.

The predicted grain size (239  $\mu\text{m}$ ) of AA6060 alloy inoculated by 0.5 kg/ton Al-3Ti-1B with a cooling rate of 1.6 K/s is slightly lower than the experimentally measured one (262  $\mu\text{m}$ ). For the alloy inoculated with a 2.0 kg/ton Al-3Ti-1B master alloy, an average grain size of 191  $\mu\text{m}$  is predicted by the model, which is slightly larger than the measured grain size, 177  $\mu\text{m}$ . Generally,

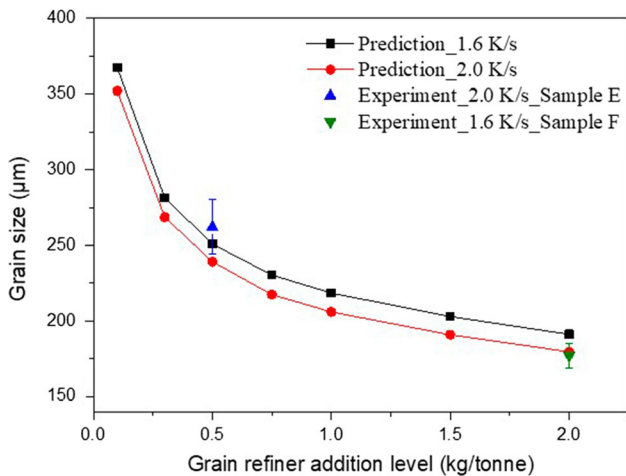


Fig. 6—Calculated grain size vs grain refiner addition level curves for a cooling rate of 1.6 K/s and 2.0 K/s and measured grain sizes for sample E and F.

the prediction results show a good agreement with the experimental results.

To show the influences of cooling rate and addition level of grain refiners on the grain size of solidified TP-1 type samples, the grain size evolution as a function of the addition level of Al-3Ti-1B master alloy has been modeled and the simulation results are summarized in Figure 6, where the experimentally measured grain sizes for sample E and F are also included as a comparison. As can be seen, the predicted grain size decreases sharply with increasing addition level of grain refiners until it reaches 0.5 kg/ton. With a further increase in the addition level, the grain size reduces, but with a slower reduction rate. The cooling rate also has a strong influence on the grain size, where 2.0 K/s cooling rate leads to obviously smaller grain sizes than with a cooling rate of 1.6 K/s.

The figure shows that the predicted grain sizes for the experimental conditions of Sample E and F are generally in good agreement with the measured grain size. Notably, no tuning was done with the input parameters for the number density and size distribution of  $\text{TiB}_2$  particles in the master alloy. It further demonstrates that the grain size prediction model based on free growth nucleation model is powerful for prediction of solidification grain size of TP-1 type test samples of inoculated aluminum alloys.

To quantitatively determine the level of potent grain refiners effectivity in the aluminum melts with addition of oxide inclusions in the form of chips before and after filtration, a reverse calculation has been done by using the grain size prediction model. The calculation results for sample A to D are shown in Table V.

The calculated effective levels of potent grain refiners in the melt before filtration are much lower than the introduced ones. For sample A and C, only 28 and 11.5 pct, respectively, of the added grain refiner particles have acted as potent particles in the melt before filtration, implying a strong interaction between the  $\text{TiB}_2$  particles and the inclusions in the melt. Furthermore, the potent grain refiner particles are further reduced after the filtration. The residual effective potent grain refiner particle level of sample B is only 0.14 kg/ton, which is 12 pct of the added value. For sample D, the residual potent grain refiners are even less, only 1 pct of what added remains active after filtration. This indicates that the filtration has substantially reduced the level of effective grain refiners in the melt, especially for the high grain refiner addition level condition. It means that massive grain refiner particles may have been

Table V. Added Grain Refiner and Calculated Active Grain Refiner Concentration Level in the Melt

Grain Size ( $\mu\text{m}$ )	Added Grain Refiner (kg/ton)	Calculated Potent Grain Refiner in Melt (kg/ton)
A: 340	0.5	0.14
B: 407	0.5	0.06
C: 286	2.0	0.23
D: 606	2.0	0.02



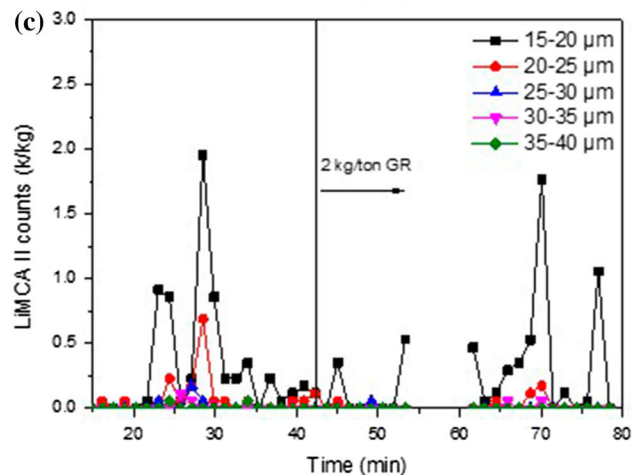
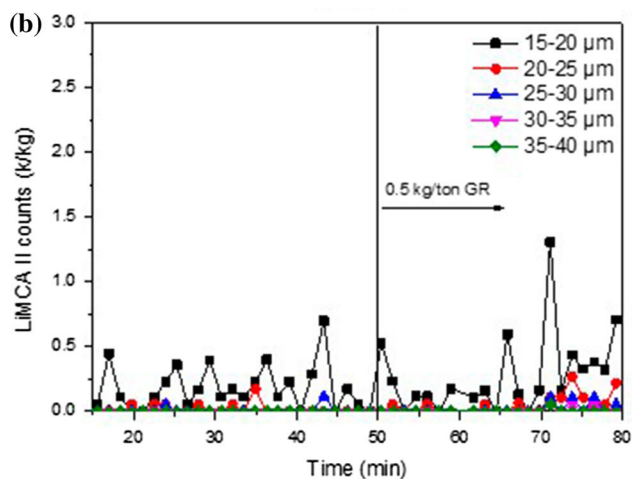
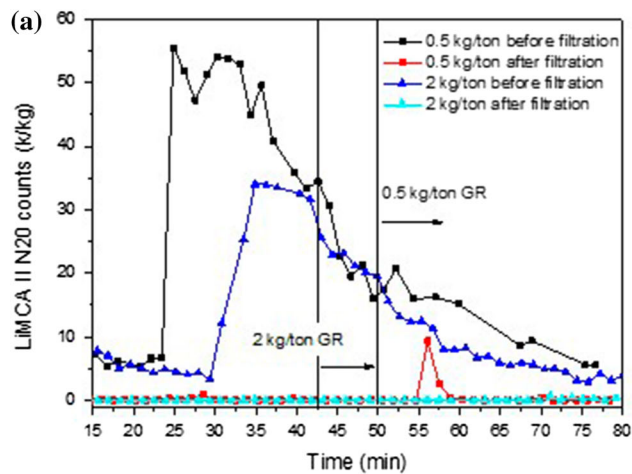


Fig. 7—N20 count results for filtration tests with a grain refiner addition level of 0.5 kg/ton and 2.0 kg/ton. (a) The inclusion counts for both before and after filtration. (b) The inclusion counts after filtration with 0.5 kg/ton GR addition, classified by the inclusion diameter sizes. (c) The inclusion counts after filtration with 2.0 kg/ton GR addition, classified by the inclusion diameter sizes. The inclusion counts for (c) at 55 to 60 min are deleted because of the PoDFA disturbing corresponding to (a). The black solid lines indicate when grain refiner is added to the melt.

captured by the filter or become inefficient nucleation sites during the filtration process.

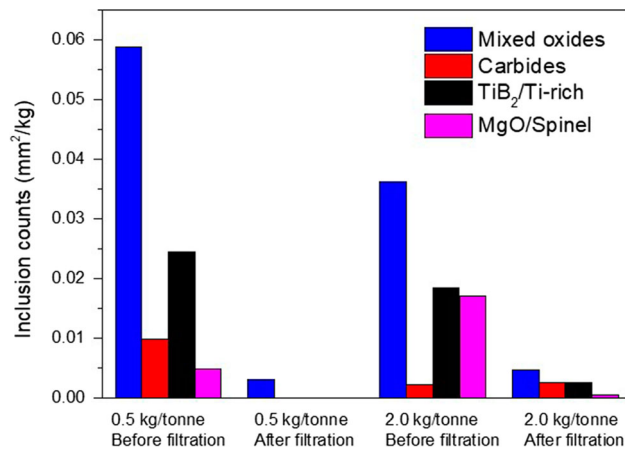


Fig. 8—Results from PoDFA samples show the inclusion concentration in the melt.

### C. Influence of GR Addition and Filtration on Inclusion Size Distribution in Melt

The counts of inclusions of different sizes in the aluminum melt before and after filtration have been measured by LiMCA II. Figure 7(a) shows the evolution of N20 values of inclusions as a function of time during the filtration loop. For the two filtration experiments, the time for the addition of Al-3Ti-1B master alloys was labeled in the figure. After filtration by 80 PPI filters, the inclusion levels in the melt are extremely low, showing that most of the inclusions have been blocked by the CFF. At the same time, at the two different addition levels of grain refiners the as-filtrated melts show the same level of inclusions, indicating the addition of the grain refiners does not affect the counts of inclusions with diameters  $> 20 \mu\text{m}$  after filtration, regardless of the grain refiner addition level. It should be noted that the sudden increase of N20 counts after filtration at 55 minutes is due to the PoDFA sampling, which disturbed the melt in the launder.

Because of the limitation of LiMCA II, the smallest inclusion size that can be detected is  $15 \mu\text{m}$ . Figures 7(b) and (c) shows the number counts for inclusions after filtration in the melt with the addition of 0.5 and 2.0 kg/ton grain refiners, respectively. The inclusions have been classified into five size classes in the range of  $15\text{--}40 \mu\text{m}$ . Except for the slight increase at 70 minutes in Figure 7(b) and the abnormal point at 55 minutes in Figure 7(c) due to the PoDFA sampling, the post filtration inclusion counts of different size classes are constantly low, regardless of the grain refiner addition and the inclusion level before filtration. Generally, the number of large inclusions is lower than for small inclusions in the as-filtrated melt. This is reasonable since the filter works better for removing larger inclusions. The results show that the 80 PPI filters have an excellent filtration efficiency, i.e., most inclusions were captured and retained in the filter.

The PoDFA samples were also taken before and after filtration. Figure 8 shows the results collected from the PoDFA analyses. Most inclusions in the melt before filtration are mixed oxides, and the remaining detected

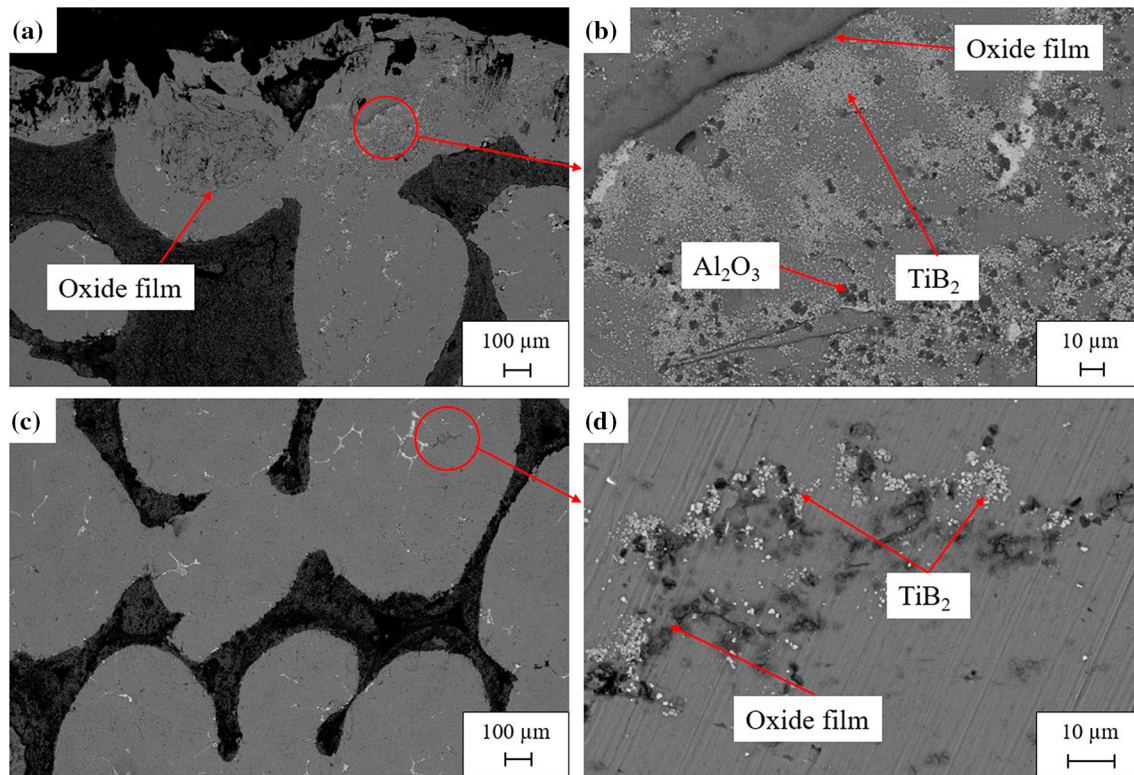


Fig. 9—Microstructure of spent filters. (a) The top region of a spent filter used for filtration of aluminum with a grain refiner addition level of 2 kg/ton, where massive inclusions can be found. (b) Enlarged area in (a) where massive  $\text{TiB}_2$  particles, oxide films, and oxide particles (black dots) can be found. (c) Central region of a spent filter used for filtration of aluminum with a grain refiner addition level of 0.5 kg/ton. Few inclusions can be found in the central region. (d) Enlarged area in (c) where grain refiner is tangled with oxide films.

inclusions include carbides,  $\text{TiB}_2/\text{Ti}$ -rich inclusions, and  $\text{MgO}/\text{spinel}$ s. As can be seen, the inclusion level in the melt is significantly reduced after the filtration. This reduction is more significant for the case where 0.5 kg/ton grain refiner is introduced. After filtration, no other inclusions but a small amount of mixed oxide inclusions can be detected. For the aluminum melt with the addition of 2.0 kg/ton grain refiners, after filtration, all four types of inclusions can be detected. The detection of the  $\text{TiB}_2/\text{Ti}$ -rich inclusions indicates that more  $\text{TiB}_2$  particles have survived from the filtration process than the melt containing 0.5 kg/ton grain refiners. By comparing the results from LiMCA measurement and TP-1 tests, it can be concluded that most of the  $\text{TiB}_2$  particles in the post-filtration melt are in the form of clusters with sizes  $< 15 \mu\text{m}$ .

#### D. Grain Refiner Particles and Inclusions in the Spent Filter

To explore how the density of potent grain refiner particles in the aluminum melt was reduced by the filtration process, the spent filters containing solidified aluminum have been examined. Figures 9(a) and (b) show the spent filter used for filtration of melt with a grain refiner addition level of 2.0 kg/ton. The black areas are the pore walls of the filter and the gray areas are solidified aluminum. As can be seen, many oxide films and inclusions accumulated at the top of the filter

(Figure 9(a)). Figure 9(b) shows an enlarged image of the labeled area in Figure 9(a). Interestingly, a huge number of  $\text{TiB}_2$  particles and oxide particles were captured by the oxide films in the top window of the spent filter.

Figure 9(c) shows the bulk region of the spent filter used for filtration of aluminum melt with 0.5 kg/ton grain refiner, and Figure 9(d) shows the enlarged area in Figure 9(c). Clusters of  $\text{TiB}_2$  particles attached to oxide film inclusions can also be observed, although the amount is less in this filter than in the previous one. This should be attributed to the different grain refiner addition levels. Generally, clusters of  $\text{TiB}_2$  particles adhering to oxide film inclusions as shown in Figure 9(d) can be found through the whole filters for both tests. However, the inclusions are more easily found in the top region. This confirms that a large fraction of the grain refiner particles has been blocked by the filter during filtration, particularly by the cake layer of the filter.

## IV. DISCUSSION

The as-cast grain size of inoculated aluminum alloys is dependent on the alloy chemistry, cooling rate, and number density of potent grain refiner particles. In the present work, all the experimental alloys have the same initial chemical composition, including Ti content and the solidification conditions, such as cooling rate and

temperature gradient, are also kept similar for all TP-1 samples. This ensures that the grain growth restriction effect by alloy chemistry remains the same while the final grain refinement is only controlled by the inclusion contents and the filtration process. The addition of a higher amount of Al-3Ti-1B master alloy may slightly increase the Ti content in the final alloy. However, since the excess Ti content in Al-3Ti-1B (the equilibrium stoichiometry for TiB<sub>2</sub> is Al-2.22Ti-1B) is much lower than the Al-5Ti-1B master alloy, the introduction of Ti into the alloys by inoculation is rather limited. Regarding the dissolving and dispersing of the grain refiner master alloys, the feeding of the grain refiner rod is a continuous process that follows the same procedure as in the industrial production line. The grain refiner addition point has a certain distance to the filter box, and the sampling points are right before and after the filter box. This ensures the grain refiner rod to be fully dissolved and dispersed in the melt. Therefore, the only variable which strongly influences the grain refinement efficiency is the number density and spatial distribution of the potent inoculant particles, TiB<sub>2</sub>. Since the experimental aluminum melt was always flowing in the loop, the chance of sedimentation of TiB<sub>2</sub> particles is low. The significant increase in grain size of the inoculated aluminum alloys after the filtration process regardless of the grain refiner addition level should be attributed to the decrease of the number of effective potent grain refiner particles. Due to the detection limit of LiMCA II (cannot detect particles < 15 μm), little is known about the removability of CFF filters on smaller particles, such as TiB<sub>2</sub> (0.5 to 5 μm<sup>[1,2]</sup>). Here, the results confirmed the good filtration ability of 80 PPI filters on smaller particles such as TiB<sub>2</sub>.

Since the average pore size of 80 PPI filter is  $383 \pm 87$  μm,<sup>[34]</sup> which is much larger than the size of TiB<sub>2</sub> particles, it is in principle difficult for the filters to block the grain refiner particles. However, when there are many oxide film inclusions in the melt, which usually have sizes in the range of 10–5000 μm,<sup>[35]</sup> oxide films can form bridges at the top region of CFF and gradually form a cake layer. Our previous works<sup>[17,36]</sup> showed that there is a strong adherence between oxide films and TiB<sub>2</sub> particles. Therefore, the cake layer can block a large fraction of the TiB<sub>2</sub> particles. In addition to the cake layer, the oxide films adhered to the pore wall inside the filter can also capture other inclusions and TiB<sub>2</sub> particles. Once the oxide films are attached to the filter by one end while the other end is floating in the melt, the effective areas of the filter for capturing inclusions increase, and thus the depth filtration mode is enhanced.

It is well known that only < 2 pct of the total TiB<sub>2</sub> particles can act as potent nucleation particles for aluminum grains.<sup>[3]</sup> An agglomeration of TiB<sub>2</sub> particles to aluminum oxide films does not necessarily reduce the grain refinement efficiency, especially when the addition level of grain refiners is high enough. However, the results in the present work show that the grain refinement efficiency is significantly reduced once a cake layer has been formed in the filter because of the high content of oxide films in the melt.

It is also found that, even without filtration, an ultra-high content of oxide films can still significantly reduce the grain refinement efficiency. This is also due to the strong adherence between TiB<sub>2</sub> particles and oxide films, as there is a large chance for the grain refiner particles to meet and agglomerate onto the oxide film inclusions in the flowing liquid metal. Such an agglomeration will lead to a reduction in number density of potent grain refiner particles because once an aluminum grain is nucleated onto one of the TiB<sub>2</sub> particles adhered on the oxide film, the neighboring TiB<sub>2</sub> particles cannot initiate new grains because of the solute segregation induced reduction of nucleation undercooling in the surrounding melt.<sup>[1,11]</sup> This is why the measured grain size of TP-1 test samples before filtration (A and C) is much larger than in sample E and F.

As shown in Table IV, the predicted grain size is generally in good agreement with the experimental results, which confirms the reliability of the grain prediction model. By the modeling work, it can be estimated that the addition of ultra-high inclusion load in the melt has reduced the number density of potent grain refiner particles by 72 and 88.5 pct for the alloys with the addition of 0.5 and 2.0 kg/ton Al-3Ti-1B master alloy, respectively. The more grain refiner particles are added into the melt, the easier it is for them to agglomerate onto oxide films, forming clusters. Therefore, the reduction in grain refinement efficiency is more significant for the case with a higher addition level of grain refiners.

Even though the grain size is increased for both tests after the filtration, a more significant increase is observed when the grain refiner addition level is higher, as shown in Figures 2 through 5. The total number of potent grain refinement particles in sample D is even smaller than in sample B, where the initial addition level of grain refiners in the former alloy is four times as high as in the latter one. This is a surprising result, which implies that the exact agglomeration behavior of TiB<sub>2</sub> particles onto oxide films is complex and needs to be further explored. It is a common industrial practice to add grain refiner master alloys before filtration during DC-casting processes, because filtration can block the large inclusion particles introduced by grain refiners, which is crucial for the surface quality of final rolling or extrusion products. However, when the aluminum melt contains a high fraction of inclusions like oxide films, the filtration and grain refinement processes have to be optimized. On the other hand, the results also suggest a potential method to remove fine particle inclusions in aluminum melt by combining a large number of oxide film inclusions with fine-pore CFF. However, as a cost, this will cause a shorter usage time of the filter. This method is also valid for TiC particles, as we have discovered that TiC particles also have strong adherence to aluminum oxide films.<sup>[36]</sup> The addition of grain refiner master alloys after the filtration process is also an option but can cause other problems. The master alloys usually contain large agglomerated TiB<sub>2</sub> particles. If they are introduced into the final casting ingot, it will significantly reduce the processing ability and the surface properties of the final aluminum products.



It should be mentioned that the present findings have been based on ultra-high inclusion load and 80 PPI filter. Even though the 80 PPI filter is rarely used in the industry nowadays because of its high pressure drops, there are more demands from the aluminum industry to use such filters with the aim of producing high-quality aluminum ingots used for aluminum cosmetic products with high surface gloss. It is critical to minimize all the possible inclusions inside the aluminum ingot, including the large  $TiB_2$  particles/agglomerates. The results obtained in this work have important implications for the aluminum industry in terms of production of high-quality DC-cast ingots for the above-mentioned high-end cosmetic aluminum products. Of course, more systematic work on the influence of lower inclusion loads and CFF filters of larger pore sizes on the grain refinement efficiency is still necessary to reach an in-depth understanding of the underlying mechanism.

## V. CONCLUSIONS

In the present work, the influences of the filtration process on grain refinement efficiency under an ultra-high inclusion load are investigated by TP-1 type solidification tests. A grain size prediction model has also been applied to calculate the solidification grain size and estimate the loss of effective grain refiner particles during the filtration. The major conclusions can be summarized as follows:

1. The filtration process does reduce the grain refinement efficiency under an ultra-high inclusion load by using an 80 PPI filter, which is more significant for an alloy with the addition of 2.0 kg/ton grain refiners than that of 0.5 kg/ton. The significant reduction of grain refinement efficiency is ascribed to the reduction in the number density of potent nucleation particles in the melt during filtration. A large fraction of  $TiB_2$  particles in the melt was found to adhere to the oxide films blocked by the filter in the cake layer.
2. Modeling calculation and experimental results show that the existence of an ultra-high level of oxide film inclusion in the melt also has reduces the grain refinement efficiency before the filtration. This has been attributed to the strong adherence between  $TiB_2$  particles and oxide films in the melt, which reduces the number density of potent nucleation sites in the alloy.
3. LiMCA II measurements show that the addition of grain refiner does not increase the number density of inclusions  $> 15 \mu m$  in the post-filtration aluminum melt during filtration by 80 PPI filter under an ultra-high inclusion load condition. However, the PoDFA test shows that with an addition of 2.0 kg/ton Al-3Ti-1B grain refiners,  $TiB_2$  particles containing inclusions ( $< 15 \mu m$ ) can still be found in the post-filtration melt.

## ACKNOWLEDGMENTS

This research was carried out as part of the Norwegian Research Council (NRC)-funded BIA-IPN Project (256724/O20) SmartAl. It includes the following partners: Hydro Aluminum AS, Hydal Aluminum Profiler AS, Hycast AS, Ekornes ASA, NTNU and SINTEF. Funding by the industrial partners and NRC is gratefully acknowledged.

## CONFLICT OF INTEREST

On behalf of all authors, the corresponding author states that there is no conflict of interest.

## FUNDING

Open access funding provided by NTNU Norwegian University of Science and Technology (incl St. Olavs Hospital - Trondheim University Hospital).

## OPEN ACCESS

This article is licensed under a Creative Commons Attribution 4.0 International License, which permits use, sharing, adaptation, distribution and reproduction in any medium or format, as long as you give appropriate credit to the original author(s) and the source, provide a link to the Creative Commons licence, and indicate if changes were made. The images or other third party material in this article are included in the article's Creative Commons licence, unless indicated otherwise in a credit line to the material. If material is not included in the article's Creative Commons licence and your intended use is not permitted by statutory regulation or exceeds the permitted use, you will need to obtain permission directly from the copyright holder. To view a copy of this licence, visit <http://creativecommons.org/licenses/by/4.0/>.

## REFERENCES

1. Y. Xu, D. Casari, R.H. Mathiesen, and Y. Li: *Acta Mater.*, 2018, vol. 149, pp. 312–25.
2. A.L. Greer, P.S. Cooper, M.W. Meredith, W. Schneider, P. Schumacher, J.A. Spittle, and A. Tronche: *Adv. Eng. Mater.*, 2003, vol. 5, pp. 81–91.
3. A. Greer, A. Bunn, A. Tronche, P. Evans, and D. Bristow: *Acta Mater.*, 2000, vol. 48, pp. 2823–35.
4. D.G. McCartney: *Int. Mater. Rev.*, 1989, vol. 34, pp. 247–60.
5. M. Easton and D. StJohn: *Metall. Mater. Trans. A.*, 1999, vol. 30A, pp. 1613–23.
6. M. Easton and D. StJohn: *Metall. Mater. Trans. A.*, 1999, vol. 30A, pp. 1625–33.
7. Z. Fan, Y. Wang, Y. Zhang, T. Qin, X.R. Zhou, G.E. Thompson, T. Pennycook, and T. Hashimoto: *Acta Mater.*, 2015, vol. 84, pp. 292–304.
8. T. Quested and A. Greer: *Acta Mater.*, 2005, vol. 53, pp. 2683–92.
9. A. Greer and T. Quested: *Philos. Mag.*, 2006, vol. 86, pp. 3665–80.

10. Q. Du and Y. Li: *Acta Mater.*, 2014, vol. 71, pp. 380–9.
11. Y. Xu, D. Casari, Q. Du, R.H. Mathiesen, L. Arnberg, and Y. Li: *Acta Mater.*, 2017, vol. 140, pp. 224–39.
12. Y. Xu, Y. Deng, D. Casari, R.H. Mathiesen, X. Liu, and Y. Li: *J. Alloys Compd.*, 2021, vol. 854, p. 155323.
13. Y. Wang, C. Fang, L. Zhou, T. Hashimoto, X. Zhou, Q. Ramasse, and Z. Fan: *Acta Mater.*, 2019, vol. 164, pp. 428–39.
14. Y. Li, B. Hu, B. Liu, A. Nie, Q. Gu, J. Wang, and Q. Li: *Acta Mater.*, 2020, vol. 187, pp. 51–65.
15. C. Limmaneevichitr and W. Eidhed: *Mater. Sci. Eng. A.*, 2003, vol. 349, pp. 197–206.
16. H. Chen, J. Jie, K. Svyarenko, H. Ma, and T. Li: *J. Mater. Res.*, 2014, vol. 29, pp. 1656–63.
17. J. Yang, S. Bao, S. Akhtar, and Y. Li: *Metall. Mater. Trans. B.*, 2021, vol. 52B, pp. 2497–508.
18. J. Cui and H.J. Roven: *Trans. Nonferr. Metal Soc.*, 2010, vol. 20, pp. 2057–63.
19. R.A. Olson and L.C. Martins: *Adv. Eng. Mater.*, 2005, vol. 7, pp. 187–92.
20. R. Wakeman and S. Tarleton: *Solid/Liquid Separation: Principles of Industrial Filtration*, 1st ed. Elsevier, New York, 2005, pp. 10–2.
21. S. Bao, *Ph.D. thesis*, Norwegian University of Science and Technology, 2011, pp. 23–25.
22. N. Towsey, W. Schneider, H.-P. Krug, A. Hardman, and N.J. Keegan: *Essential Readings in Light Metals: Volume 3 Cast Shop for Aluminum Production*, Springer, New York, 2016, pp. 291–5.
23. N. Towsey, W. Schneider, H.-P. Krug, A. Hardman, and N.J. Keegan: *Continuous Casting*, Wiley, New York, 2006, pp. 26–32.
24. S. Ray, B. Milligan, and N. Keegan: *Aluminium Cast House Technology*, STAS Inc., Chicoutimi, 2005, pp. 1–12.
25. J. Yang, S. Bao, S. Akhtar, U. Tundal, S. Tjøtta, and Y. Li: *Metall. Mater. Trans. B*, 2021, vol. 52, pp. 3946–60.
26. Tundal U., Steen I., Strømsvåg Å., Haugen T., Fagerlie J.O., Håkonsen A. (2019) Drain Free Filtration (DFF)—A New CFF Technology. In: Chesonis C. (eds) *Light Metals 2019. The Minerals, Metals & Materials Series*. Springer, Cham. [https://doi.org/10.1007/978-3-030-05864-7\\_134](https://doi.org/10.1007/978-3-030-05864-7_134).
27. Aluminum Association: *Standard Test Procedure for Aluminum Alloy Grain Refiners 2012*, Aluminum Association, Arlington County, 2012.
28. Y. Xu, Y. Deng, D. Casari, R.H. Mathiesen, X. Liu, and Y. Li: *J. Mater. Sci.*, 2020, vol. 55, pp. 15621–35.
29. Y. Xu, Q. Du, and Y. Li: *Trans. Indian Inst. Met.*, 2015, vol. 68, pp. 1013–6.
30. H. Men, B. Jiang, and Z. Fan: *Acta Mater.*, 2010, vol. 58, pp. 6526–34.
31. Qested, T.E.: *Solidification of Inoculated Aluminium Alloys*, University of Cambridge, Cambridge, 2004.
32. M. Martorano, D. Aguiar, and J. Arango: *Metall. Mater. Trans. A.*, 2015, vol. 46A, pp. 377–95.
33. D. Shu, B. Sun, J. Mi, and P.S. Grant: *Acta Mater.*, 2011, vol. 59, pp. 2135–44.
34. M.W. Kennedy, K. Zhang, R. Fritzsche, S. Akhtar, J.A. Bakken, and R.E. Aune: *Metall. Mater. Trans. B.*, 2013, vol. 44B, pp. 671–90.
35. L.J. Gauckler, M.M. Waeber, C. Conti, and M. Jacob-Dulière: *Essential Readings in Light Metals: Volume 3 Cast Shop for Aluminum Production*, Springer, Cham, 2016, pp. 251–62.
36. J. Yang, S. Bao, S. Akhtar, P. Shen, and Y. Li: *Metall. Mater. Trans. B.*, 2021, vol. 52B, pp. 382–92.

**Publisher's Note** Springer Nature remains neutral with regard to jurisdictional claims in published maps and institutional affiliations.